Millimetre and submillimetre molecular line observations of the southwest lobe of L 1551 - evidence of a shell structure

Astron. Astrophys. 179, 237–248 (1987)

ASTRONOMY
AND
ASTROPHYSICS

Millimetre and submillimetre molecular line observations of the southwest lobe of L 1551: evidence of a shell structure

Ruth Rainey[1], Glenn J. White[1], K.J. Richardson[1], M.J. Griffin[1], N.J. Cronin[2], T.S. Monteiro[3], and J. Hilton[4].

[1] Astrophysics Group, Department of Physics, Queen Mary College, University of London, Mile End Road, London E1 4NS, England
[2] School of Physics, University of Bath, Claverton Down, Bath BA2 7AY, England
[3] Department of Physics, University of Durham, Science Laboratories, South Road, Durham, DH1 3LE, England
[4] Department of Mathematical Sciences, Goldsmiths' College, University of London, New Cross, London SE14 4NW, England

Received September 30, accepted December 2, 1986

Summary. Observations have been made of the southwest outflow lobe of L 1551 in several millimetre and submillimetre molecular lines. Maps have been made in the $J = 3$–2 and $J = 2$–1 transitions of CO over areas of 7.5 by 2.5 arcmin and 5 by 5 arcmin respectively, using the 3.8 m United Kingdom Infrared Telescope (UKIRT). Higher angular resolution maps have also been made in the $J = 2$–1 CO transition over an area of about 6 by 3.5 arcmin with the NRAO 12 m telescope, and additional observations of the $J = 4$–3 transitions of HCN, HCO^+ and $H^{13}CO^+$ were obtained towards selected positions. The detection of the $J = 4$–3 transitions of HCN, HCO^+, and $H^{13}CO^+$ close to the position of HH 29 suggests the presence of very dense gas in this region ($n > 10^5\,cm^{-3}$), although LVG analysis of the CO line wings suggests a density of only $3\,10^3$ to $10^4\,cm^{-3}$. To the southwest of HH 29 there is a decrease in both the linewidth and intensity of CO emission. This may result from an interaction between the outflowing gas and a dense clump of gas and may be directly related to the processes resulting in HH 29. The maps of the CO $J = 3$–2 and CO $J = 2$–1 emission integrated over various velocity intervals show evidence for a shell structure which delineates the edge of the outflow cavity. At higher blueshifted velocities the CO $J = 2$–1 and $J = 3$–2 emission is predominantly emitted from areas closer to the outflow axis. Redshifted emission from the northern edge of the shell may be a consequence of rotation of the outflowing gas. Our observations, showing a shell structure, an accelerating outflow and possible rotation of the outflowing gas, suggest that the Sweeping-Magnetic-Twist model of Uchida and Shibata (Uchida et al., 1986, and references therein) is the most appropriate of currently available models of bipolar sources, to explain the L 1551 bipolar outflow.

Key words: interstellar medium: molecular clouds – bipolar outflows

1. Introduction

The molecular outflow phase is a common stage in the early evolution of stars, and has now become a widely observed physical process. The outflow associated with L 1551 is the archetype of these bipolar molecular outflow sources. Early observations of this source by Knapp et al. (1976) showed the presence of broad asymmetric wings on the CO profiles, and subsequently it was recognised as the first bipolar molecular outflow source by Snell et al. (1980). The outflow is situated at the southeast edge of the L 1551 dark cloud complex (Sandqvist and Bernes, 1980) which is assumed to lie at a distance of 160 pc (Snell, 1981). The LSR velocity of the ambient cloud material is $\sim 6.7\,km\,s^{-1}$ (Sandqvist and Bernes, 1980), and it extends over an area of about 40′ by 40′ (Snell, 1981). In the CO $J = 1$–0 transition the molecular outflow consists of a lobe of blueshifted emission to the southwest and a lobe of redshifted emission to the northeast (Snell et al., 1980). Both lobes are highly collimated and extend over several arc minutes.

The L 1551 region has been extensively studied at optical, infrared and radio wavelengths. At the centre of the outflow is the infrared source IRS 5 (Strom et al., 1976) which has a total bolometric luminosity of 32 to 38 $L_\odot$ (Emerson et al., 1984, Cohen et al. 1984). This would imply the presence of a dust embedded pre-main sequence (PMS) star of about 1 $M_\odot$. From infrared photometry at wavelengths between 1.2 and 19 μm, Cohen and Schwartz (1983) have found that IRS 5 is extended on the scale of a few arc seconds. Infrared polarisation observations of Nagata, Sato and Kobayashi (1983) and by Hodapp (1984) suggest the presence of a thick disc whose axis lies parallel to the direction of the molecular outflow. Optical spectroscopy of the reflection nebulosity which lies close to the embedded infrared source indicates that IRS 5 has a spectral type G–K, and that its spectrum is similar to stars of the FU Ori class (Mundt et al., 1985). Strom et al. (1985) report observations at 2 μm wavelength of the region around IRS 5, which they interpret as due to light scattered from dust grains in a thick disk of about 1000 AU diameter.

Radio continuum observations of the IRS 5 area have been made by Cohen et al., (1982), Bieging et al., (1984), Snell et al. (1985) and Bieging and Cohen (1985). These studies show the central core with two jets extending 14 and 10 arcsec to the northeast and southwest of IRS 5 respectively, along the axis of the molecular outflow (Snell et al., 1985). The central core has been resolved into two point like sources separated by 0.3 arcsec (Bieging and Cohen, 1985) and they suggest that IRS 5 may contain a binary system whose orbital plane lies in a north–south direction. Another possibility is that the binary structure seen in the 15 GHz

Send offprint requests to: G.J. White

emission arises from enhancements in the ionized gas column density at the inner edge of the dense molecular disk detected by Kaifu et al. (1984), as has been suggested for the double 6 cm radio continuum source in G35.2N (Dent et al., 1985, and references therein), and subsequently for L 1551 by Rodriguez et al. (1986). At 5 GHz Bieging and Cohen (1985) have observed the radio continuum jets close to IRS 5 and they find the width of the jet to be less than 0.3 arcsec. In these observations the jet extends 3.2 arcsec with position angle 255° compared to a position angle of about 225° for the molecular outflow and the more extended radio jets.

An optical jet, coincident with the southwest radio jet, has been observed by Mundt and Fried (1983). This extends 17 arcsec southwest from IRS 5. The jet contains several emission knots connected by fainter diffuse emission. No optical jet counterpart is observed to the northeast of IRS 5, probably as a consequence of greater optical extinction in this direction. The emission knots in the jet have radial velocities which decrease from $-210\,\mathrm{km\,s^{-1}}$ (at distances between 3 and 10 arcsec from IRS 5) to $-80\,\mathrm{km\,s^{-1}}$ (between 10 and 18 arcsec from IRS 5) (Sarcander et al., 1985).

The optical jets, radio jets and the CO bipolar outflow show structure on a wide range of scales extending in a northeast–southwest direction. Three Herbig-Haro objects lie in projection against the southwest lobe of the molecular outflow. Two of these, HH 28 and HH 29, lie close to the axis of the outflow. Observations of their proper motions, when projected back along their paths, intersect close to the position of IRS 5 (Cudworth and Herbig, 1979). HH 102 (S239) is a larger area of nebulosity lying to the west of IRS 5 and is mainly a reflection nebula (Mundt et al., 1985). CCD images of a 4 by 7 arcmin region around IRS 5 have been obtained through V, R, I and H_α filters by Snell et al. (1985). These show that towards HH 102 the light from the shock excited gas and the scattered light mainly arise in different areas. The scattered light appears to delineate the walls of a cavity extending from the tip of a jet-like feature originating from IRS 5 and the shock excited gas mainly lies inside this cavity.

The bipolar molecular outflow has been studied extensively. The first observations of L 1551 in the CO $J = 1$–0 transition showed broad, low intensity wings (Knapp et al., 1976). Subsequent observations include mapping of the outflow in the CO $J = 1$–0 line by Snell et al., (1980), Snell and Schloerb (1985) and Uchida et al. (1986), and in the CO $J = 2$–1 line by Levreault (1985). Both CO transitions show the flow to be highly collimated and to extend over about 1.2 pc (~25 arcmin). Higher angular resolution observations of the CO $J = 1$–0 transition along the axis of the outflow have been made by Fridlund et al. (1984) with the Onsala 20 m telescope. These show an apparent acceleration of the outflowing gas. The outflow region has also been mapped in th 1667 MHz OH transition (Mirabel et al., 1985), the $(J, K) = (1, 1)$ inversion transition of ammonia at 23.7 GHz (Torrelles et al. 1983, Menten and Walmsley 1985) and the $J = 1$–0 and $J = 2$–1 transitions of CS (Snell and Schloerb 1985, Kaifu et al., 1984 and Batrla and Menten 1985). These observations reveal the presence of dense gas around IRS 5 which, according to the interpretation of the CS $J = 1$–0 observations by Kaifu et al. (1984), is in the form of a slowly rotating disk. However the CS $J = 1$–0 observations of Batrla and Menten (1985) did not detect a systematic velocity gradient along a line at position angle 330° or in the north-south direction. There is a considerable amount of velocity and spatial structure within the outflow, as is shown by a series of CO $J = 1$–0 spectra observed along the axis of the flow by Fridlund et al. (1984), observations of the CO $J = 1$–0 transition during a lunar occultation which gave a synthesised beamwidth of 7 arcsec (Snell and Schloerb, 1985) and the higher resolution (HPBW = 15 arcs) mapping of the outflow made by Uchida et al. (1986).

In this paper we report observations of the southwest lobe of the bipolar molecular outflow in both the $J = 2$–1 and $J = 3$–2 transitions of CO. These were made in order to investigate the structure and physical conditions within this part of the outflow. Observations of the $J = 4$–3 transitions of HCO^+, $H^{13}CO^+$, and HCN were also made towards selected positions to sample and characterise the properties of the denser gas.

2. Observations

The observations were carried out using the 3.8 m United Kingdom Infrared Telescope (UKIRT) on Mauna Kea, Hawaii, during the periods 1983 August to September, 1984 August and 1984 October. Further observations of the CO $J = 2$–1 transition were made with the 12 m National Radio Astronomy Observatory (NRAO) telescope during 1985 May.

At UKIRT the QMC submillimetre heterodyne receiver (White et al., 1986a) was operated at the cassegrain focus of the telescope. The total noise temperatures were typically 250 K at 230 GHz and 350 K at 346 GHz, including all optics, telescope and atmospheric losses. The weather conditions were generally excellent during the 1983 observing periods but somewhat worse during 1984. Pointing was determined by peaking on continuum emission from Jupiter, Saturn and Venus. Absolute pointing, as determined with an on-axis TV guider, was found to have an uncertainty of less than about 5 arcsec. Calibration was carried out at approximately 10 to 15 min intervals using a chopper wheel calibration technique. The results are given in terms of the corrected antenna temperature, T_r^* (Kutner and Ulich, 1981), where the forward spillover efficiency (η_{fss}) was estimated to be 0.9 at 346 GHz and 0.85 at 230 GHz. The beam sizes of the telescope were measured to be 55 and 83 arcsec at 346 and 230 GHz respectively, which correspond to linear sizes of 0.04 and 0.06 pc. All observations were made with respect to a reference 'off' position at Right Ascension (1950) $4^h36^m40^s$, Declination (1950) $+18°01'52''$ determined to be free of significant molecular emission. All offsets in this paper are given relative to Right Ascension (1950) $4^h28^m40^s$, Declination (1950) $+18°01'52''$, which is about 10 arcsec north of IRS 5.

At the NRAO 12 m telescope a dual channel cryogenic receiver was used. The telescope beam size was measured to be 30 arcsec (0.02 pc) and the forward spillover efficiency was estimated to be 0.73. The total system noise temperature was typically 1000–2000 K including losses due to atmospheric attenuation and dish efficiency.

3. Results

3.1. *UKIRT observations*

A region extending over 7.5 by 2.5 arcmin was mapped in the CO $J = 3$–2 transition with a spacing of 30 arcsec. This area covers most of the southwest CO lobe seen in the maps of Snell and Schloerb (1985) and a small part of the northeast lobe. In Fig. 1 we show a map of the total integrated emission, and a

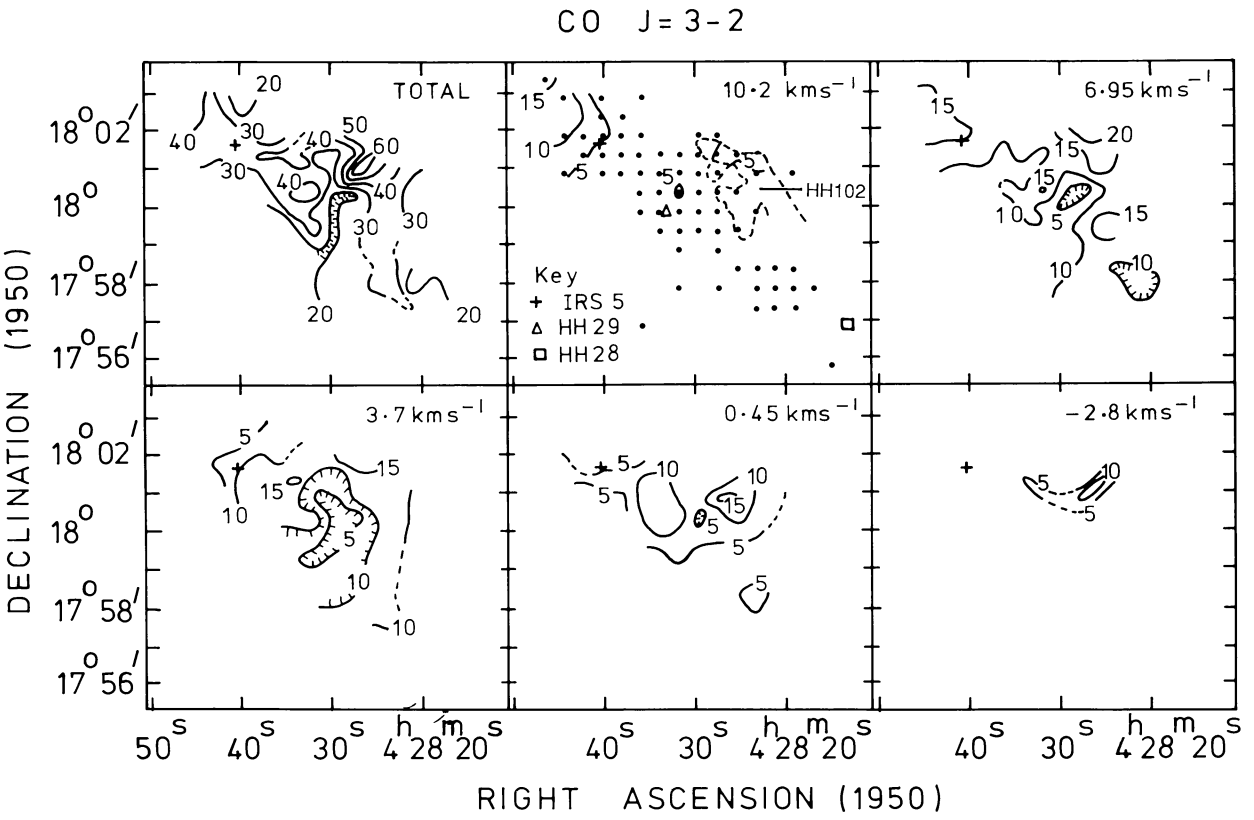

Fig. 1. Maps of the total integrated CO $J = 3$–2 emission (K km s^{-1}) in L 1551 and the CO $J = 3$–2 emission integrated in 3.25 km s^{-1} intervals. The central velocity of the relevant interval is given on each map. HH 102 is outlined by a broken line and the positions towards which spectra were obtained are marked with a dot on the 10.2 km s^{-1} map

sequence of maps of the emission integrated over 3.25 km s^{-1} velocity intevals. The total integrated CO emission shows two main peaks 30 arcsec to the north of HH 29 and towards the northeast part of HH 102. About one arcmin to the southwest of HH 29 there is a region where the total integrated emission is low, which shows an elongation perpendicular to the outflow axis, and extends as far as the southeast edge of HH 102.

The individual 3.25 km s^{-1} maps show that the region of strongest redshifted emission (i.e. at velocities contained in the map centred at 10.2 km s^{-1}) lies to the northeast of IRS 5, which is part of the northeast outflow lobe. There is also emission at redshifted velocities relative to the ambient gas over the northeastern part of HH 102. In the map centred at 3.7 km s^{-1} a shell-like structure is seen, which extends northeast from HH 29 towards IRS 5 and then bends in a westward direction to follow the shape of the cavity shown up by HH 102. The most intense emission in this velocity interval comes from two areas, one to the north of HH 29, close to IRS 5, and the other to the north of HH 102. In the map centred at 0.45 km s^{-1} the emission is concentrated in two main peaks, one lying to the north of HH 29 while the other is to the east of HH 102.

In the CO $J = 2$–1 transition an area of about 5 by 5 arcmin of the southwest lobe was mapped with a one arcmin spacing using UKIRT. The map of total integrated emission is shown in Fig. 2. We also show a series of maps of the emission integrated in velocity intervals which match those of the CO $J = 3$–2 data shown previously. The total integrated emission is most intense to the north and west of the area mapped, and in particular towards HH 102. The integrated emission to the south of HH 29 again shows a minimum, but this is neither as pronounced nor as extensive as the corresponding minimum at the same position in the CO $J = 3$–2 total integrated emission map in Fig. 1.

In the maps of emission integrated in 3.25 km s^{-1} intervals shown in Fig. 2 it can be seen that, as with the CO $J = 3$–2 transition, emission at velocities redshifted relative to the ambient gas comes mainly from the HH 102 region. In the map centred at 3.7 km s^{-1} the most intense emission is observed to come from an area lying between 30 to 60 arcsec southwest of IRS 5, from the HH 102 region, and also from an area lying 5 arcmin southwest of IRS 5, which is between HH 28 and HH 29. The shell-like structure seen in the corresponding map for the CO $J = 3$–2 transition in Fig. 1 is apparent. In the map centred at 0.45 km s^{-1} the most intense CO $J = 2$–1 emission comes from an area approximately 3 arcmin in diameter which lies between HH 29, HH 102 and IRS 5. When the effects of the larger beam size for the CO $J = 2$–1 observations are taken into account, the map of integrated emission at 0.45 km s^{-1} is similar to the corresponding map for the CO $J = 3$–2 transition.

In Fig. 3 we show a series of UKIRT CO $J = 2$–1 spectra observed along a strip in Right Ascension, which were obtained with a declination offset one arcmin south of the reference position. At the position 1'S 2'W of this position (subsequently we refer to positions such as this as 1S 2W) (Fig. 3b) the emission of the blue shifted wing is as intense as that of the gas at the ambient cloud velocity. At positions further west, the intensity of emission from material at the ambient cloud velocity increases. Spectra observed towards positions which lie on the shell-like structure seen in the 3.7 km s^{-1} map of Fig. 1 are presented in Figs. 3a

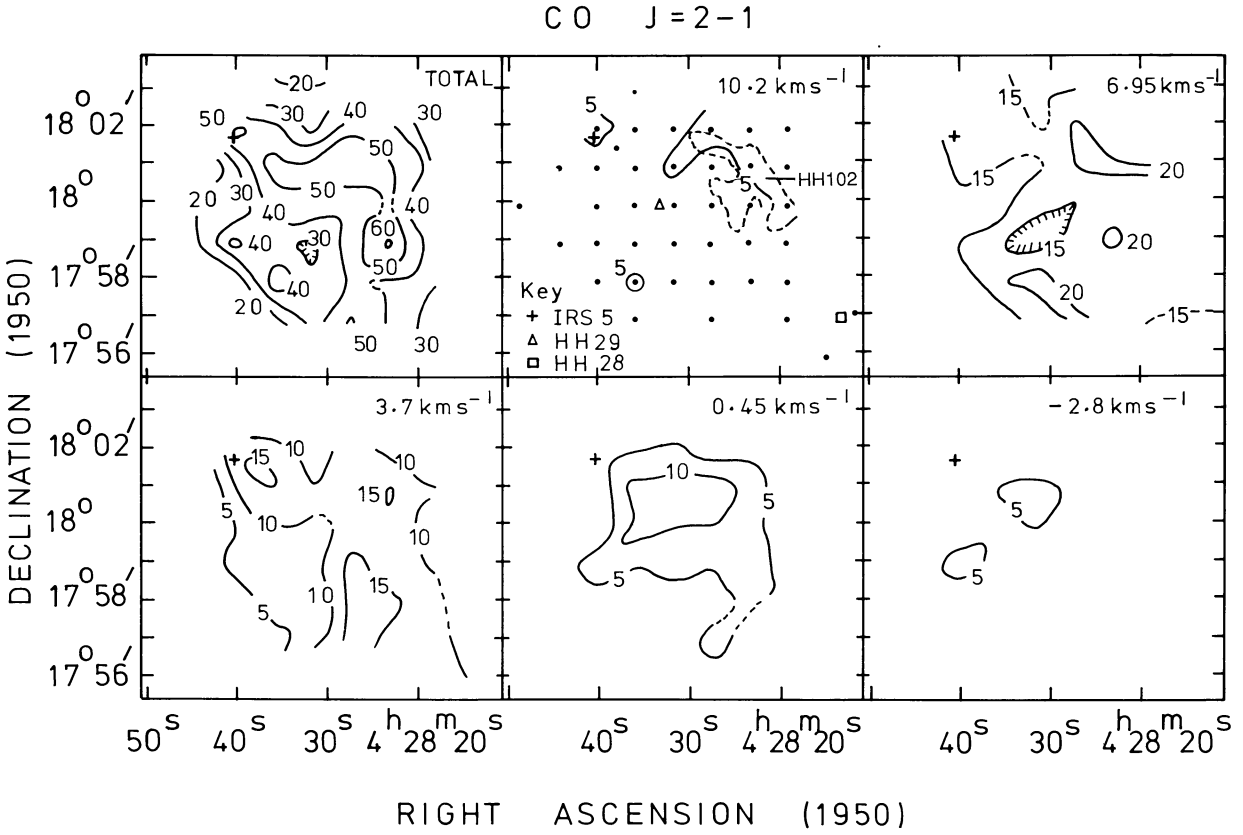

Fig. 2. Maps of the CO $J = 2$–1 emission in L 1551 observed at UKIRT. Details as for Fig. 1

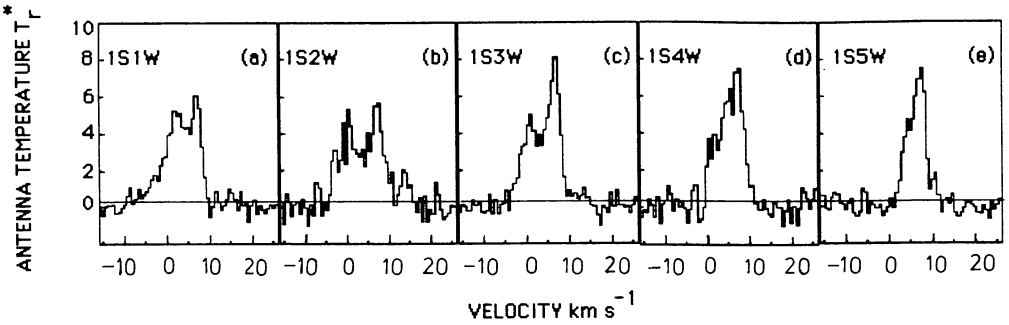

Fig. 3. A strip of five CO $J = 2$–1 spectra in the southwest outflow lobe of L 1551 observed at UKIRT. Positions are given in arcmin offset from Right Ascension (1950) = $04^h28^m40^s$, Declination (1950) = $+18°01'52''$

and 3d. In Fig. 3c we show a spectrum obtained towards a position lying close to HH 102, where intense integrated emission at 0.45 km s^{-1} in both CO $J = 3$–2 and CO $J = 2$–1 transitions is seen.

In Fig. 4 we show $J = 2$–1 and $J = 3$–2 CO spectra obtained at UKIRT towards seven positions along the southern outflow axis. The intensity of emission at the ambient cloud velocity is generally greater in the CO $J = 2$–1 spectra. There is a decrease in the intensity of CO $J = 2$–1 and $J = 3$–2 emission at 2S 2W (close to HH 29), and again at 6S 6W (one arc minute south of HH 28). The intensity of the CO $J = 2$–1 emission is always greater than the intensity of the CO $J = 3$–2 emission at the ambient cloud velocity to within the noise level. Generally the shape and intensity of the blueshifted wings in the $J = 3$–2 and $J = 2$–1 transitions are very similar, but there is a tendency for the CO $J = 2$–1 emission to be more intense at velocities above 3 km s^{-1}. A ratio of the intensity of the CO $J = 3$–2 to CO $J = 2$–1 transitions of greater than 1 may be due to the presence of optically thin gas. A ratio equal to or less than 1 could result from either optically thick gas or incomplete thermalisation of the upper level of the molecules. Since the ratio is found to be less than or equal to 1 towards most of the positions observed, and the effect of any difference in the coupling efficiencies to the beam at the two frequencies will be to reduce this ratio further, we can conclude that the gas in the outflow is generally either optically thick or the CO $J = 3$ level is not fully thermalised due to either a low kinetic temperature or low gas density.

The CO $J = 2$–1 and $J = 3$–2 lines with the greatest linewidth to the 1 K level are emitted from a region lying close to the position of HH 102. The width of the CO $J = 2$–1 line decreases

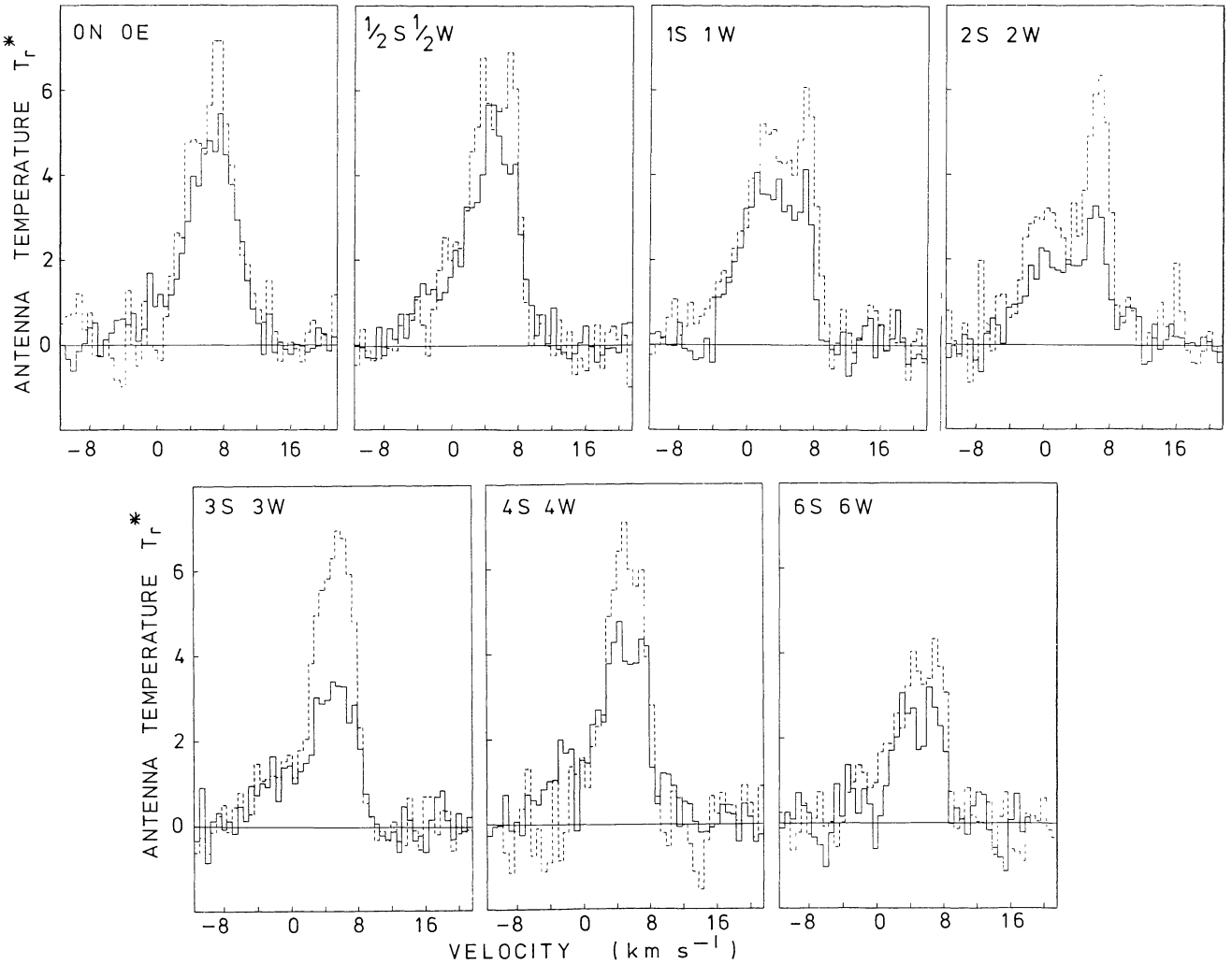

Fig. 4. CO $J = 2$–1 (–) and CO $J = 3$–2 (M) spectra observed at UKIRT towards the sourthern outflow axis of L 1551. Offsets as for Fig. 3.

from about 10 to less than 5 km s^{-1} towards a position lying about 45 arcsec south of HH 29. The CO $J = 3$–2 lines are generally broad with widths exceeding 9 km s^{-1} to the 1 K level along the southern outflow axis, except for a decrease in line width one arcmin to the southwest of HH 29. The broadest line is the CO J = 2–1 transition, with a width of 15 km s^{-1} to the 1 K level, was observed towards the position 1S 2W.

The highest peak antenna temperature occurs to the northeast of HH 102 in both the $J = 3$–2 and $J = 2$–1 transitions of CO. Both transitions also show low values of peak antenna temperature to the southwest of HH 29. In the CO $J = 3$–2 transition the antenna temperature of the high velocity gas exceeds the antenna temperature at the ambient cloud velocity in three places. The two regions where the peak antenna temperature occurs at velocities less than 2 km s^{-1} are at about 30 arcsec north of HH 29 and in a narrow region extending for 1.5 arcmin in a northwest direction from a point 45 arcsec west of HH 29, where there is also a decrease in the total integrated emission, peak antenna temperature and line width.

With UKIRT we have also detected the $J = 4$–3 transitions of HCO^+, $H^{13}CO^+$ and HCN towards a number of positions in the southwest lobe of L 1551. In Table 1 details of the detections and non-detections are given, and in Fig. 5 examples of the spectra observed are shown. At the reference position, the $J = 4$–3 transitions of HCO^+ and HCN were detected but the $H^{13}CO^+$ line was not present at a level > 0.1 K giving a lower limit on the ratio of the HCO^+ to $H^{13}CO^+$ emission of 12 ± 4. At 2S 2W, close to the position of HH 29, all three $J = 4$–3 transitions were detected and the peak antenna temperatures occurred at velocities in the range 1 to 3 km s^{-1}. These correspond to velocities blueshifted by 4 to 6 km s^{-1} with respect to the ambient cloud velocity, which is similar to the velocities at which the blueshifted wing peaks in the CO $J = 2$–1 and $J = 3$–2 lines at this position. The ratio of the peak antenna temperatures of the HCO^+ to $H^{13}CO^+$ transitions is about 7 ± 1.5 at this position, which is much greater than the usually assumed isotopic abundance ratio of 40 to 90 (the solar system value), and suggests that the HCO^+ $J = 4$–3 line is optically thick. All the HCO^+ lines detected have a full width to the 0.1 K level of greater or equal to 8 km s^{-1} with the broadest line, which has a full width of 15 km s^{-1}, being observed at 4S 4W. The HCO^+ $J = 4$–3 transition was detected towards all points along the outflow axis that were observed but not towards the positions 1S and 1W. This indicates that the material from which the HCO^+ $J = 4$–3 emis-

Table 1

Line	Position	T_r^* (K)	V_{LSR} (km s^{-1})	ΔV (to 0.1 K)	$\int T_r^* dv$ (K km s^{-1})
HCO^+ $J = 4–3$	0N 0E	1.2	6	10	5.7
	1S 1W	1.2	2	8	6.1
	2S 2W	1.6	1	13	10.3
	4S 4W	2.2	3	16	16.3
	0S 1W	<1.2	–	–	–
	1S 0W	<0.4	–	–	–
$H^{13}CO^+$ $J = 4–3$	0N 0E	<0.1	–	–	–
	2S 2W	0.2	1	7	1.5
HCN $J = 4–3$	0N 0E	0.4	5	4	0.9
	2S 2W	0.7	3	5	2.7

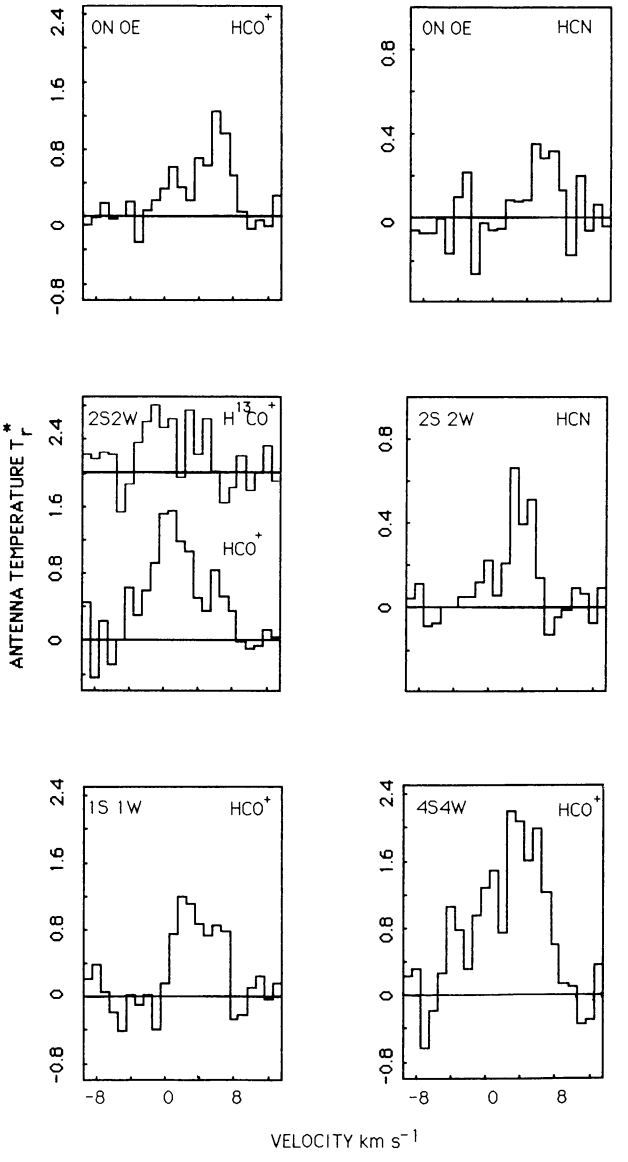

Fig. 5. Spectra of the $J = 4–3$ transitions of HCN, HCO^+ and $H^{13}CO^+$ ($\times 2.5$) towards selected positions in the southwest outflow lobe of L 1551. Offsets as for Fig. 3

sion arises is associated with IRS 5 and its molecular outflow and not with the general ambient gas.

3.2. NRAO 12 m COJ = 2–1 observations

An area of extending over about 6 by 3.5 arcmin was mapped with a 30 arcsec spacing. Figure 6 shows a map of the total integrated emission obtained from these data together with maps of the emission which has been integrated over 3.25 km s^{-1} intervals centred on velocities as close to those of the UKIRT data in Figs. 1 and 2 as was possible. There are strong similarities between the maps of the CO $J = 3–2$ UKIRT emission and the corresponding maps of Fig. 6. The main exceptions are the greater extent of the redshifted emission to the north of the area mapped in Fig. 6, which was not mapped in the CO $J = 3–2$ transition, and in the map at about 0 km s^{-1} there are still two maxima of integrated emission but these occur 30 and 60 arcsec further south in Fig. 6 than in the corresponding CO $J = 3–2$ map in Fig. 1. The maps of integrated emission centred at about -3 km s^{-1} in Figs. 1 and 6 are not similar.

In Fig. 6 it can be seen that emission comes from different areas which show considerable dependence on the velocity. At velocities redshifted relative to the ambient cloud velocity the integrated emission lies in an arc principally to the north and west of HH 29, and shows an extension to the north of IRS 5. At the ambient cloud velocity this arc is also seen and in the 3.5 km s^{-1} map it has developed into a clearly defined shell extending to the east of HH 29. There is no extension to the north of IRS 5 at this velocity. The observed shell thickness at half maximum intensity, corrected for dilution of the beam, is between 0.03 to 0.07 pc (42 to 90 arcsec). A minimum in the integrated emission is centred on a position about 35 arcsec northeast of HH 29. In the next map centred at 0.3 km s^{-1} the shell structure is no longer visible, instead two peaks are seen which lie within the shell structure seen in the map centred at 3.5 km s^{-1}. The minimum that lies between these two peaks again comes from a position about 35 arcsec northeast of HH 29. In the map centred at -3.0 km s^{-1} this has become the position of the single emission peak.

The CO $J = 2–1$ spectra observed at the NRAO 12 m telescope are generally similar in shape to those observed at UKIRT in the CO $J = 2–1$ transition except that the emission at the

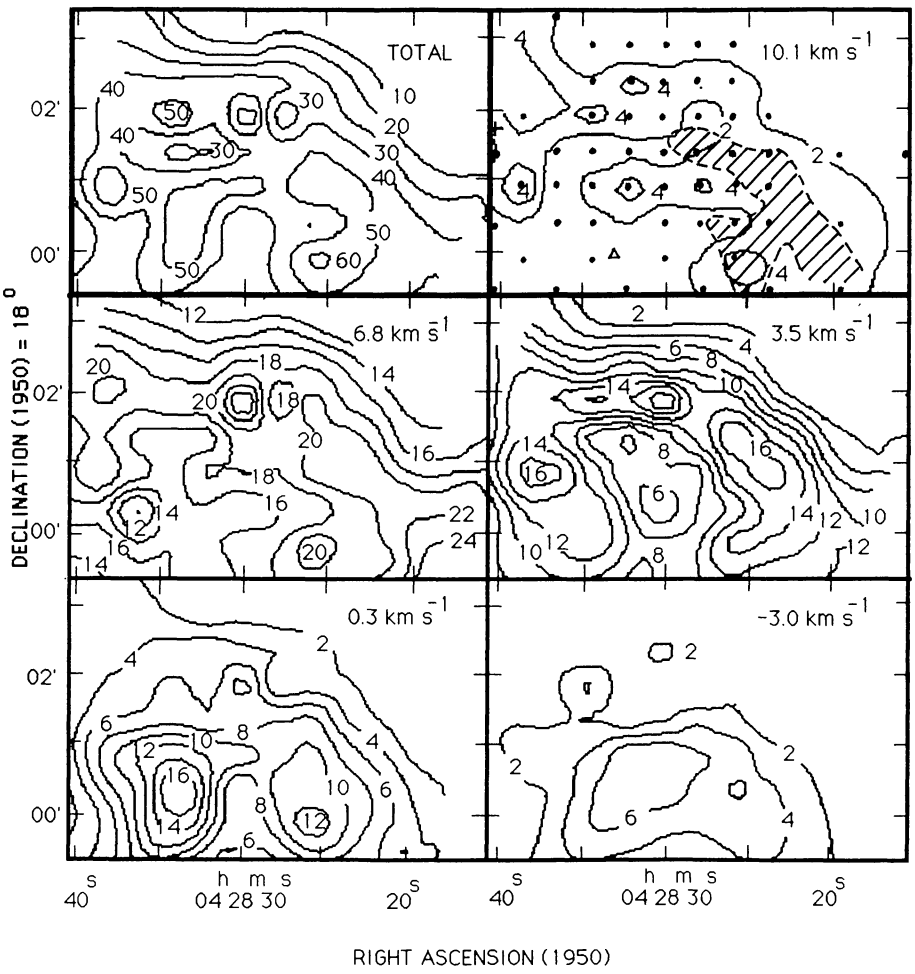

Fig. 6. Maps of the CO $J = 2$–1 emission in L 1551 observed at the NRAO 12 m telescope. Details as for Fig. 1. HH 102 is indicated by the shaded region on the 10.1 kms^{-1} map and the positions of IRS 5(+) and HH 29(Δ) are also marked.

ambient cloud velocity, in terms of T_r^*, tends to be more intense for the NRAO observations. Examples of spectra observed at the NRAO are shown in Fig. 7. These were observed towards similar positions as four of the UKIRT CO $J = 2$–1 spectra shown in Fig. 3.

4. Discussion

In L 1551 collimation appears to occur on many scales from less than 0.01 pc (optical and radio jets) to greater than 0.5 pc (the molecular outflow). Several models have been proposed to account for the collimation of the bipolar outflows and these are summarised in the review paper by Strom and Strom (1985). Our observations are of the larger scale properties of the outflow.

Snell et al. (1985) suggest that the reflection nebulosity in the HH 102 region delineates the "walls" of a cavity formed by the interaction of a collimated stellar wind with the ambient molecular cloud. The CO $J = 1$–0 observations of Snell and Schloerb (1985) support this, in particular their lunar occultation measurements which identify two points of low velocity emission ($V_{lsr} = 2$

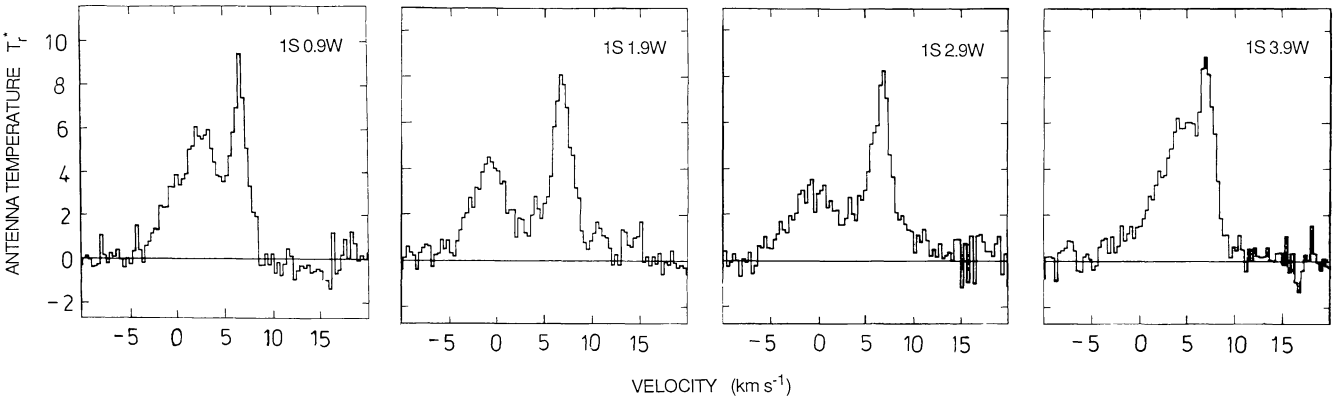

Fig. 7. A strip of four CO $J = 2$–1 spectra in the southwest outflow lobe of L 1551 observed at the NRAO 12 m telescope. Offsets as for Fig. 3

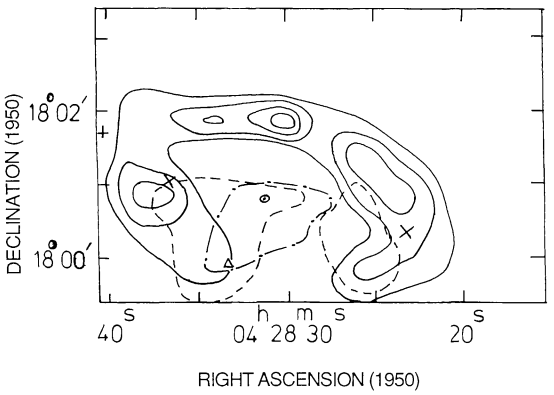

Fig. 8. The shell structure seen in the NRAO 12 m telescope data. Contours have been taken from the maps shown in Fig. 7 centred at 3.5 km s^{-1}(—), 0.3 km s^{-1}(– – –) and −3.0 km s^{-1}(–·–). Other points of interest are IRS 5(+), HH 29 (Δ) and the positions of low (×) and high (o) velocity emission from the lunar occultation measurements of Snell and Schloerb (1985)

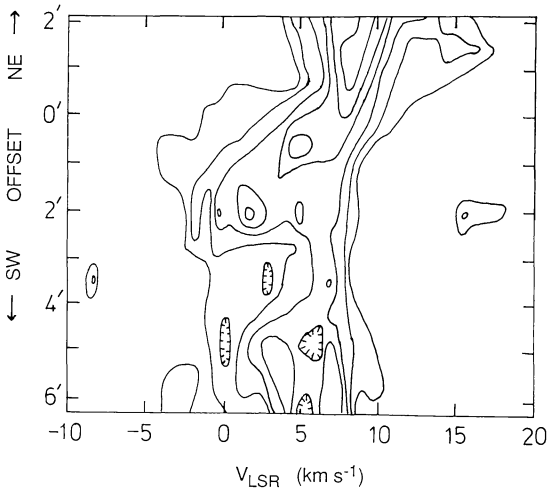

Fig. 9. Position-velocity plot of the CO $J = 3$–2 emission in L 1551 along the outflow axis. Offsets are given in arc minutes relative to Right Ascension (1950) = $04^h28^m40^s$, Declination (1950) = +18°01′52″. Contours are at 1 K intervals with the lowest contour at 1 K

to 5 km s^{-1}), each with a width of less than 0.03 pc (40 arcsec). This is the same as the minimum thickness that we find for the shell. These positions are suggested to lie on opposite edges of a shell which is seen for the first time in the present maps of integrated CO $J = 2$–1 emission, particularly at 3.5 km s^{-1} in Fig. 6. The shell structure and these positions are diagramatically illustrated in Fig. 8 together with the position of the spatially extended high velocity emission ($V_{lsr} = -3$ to 1 km s^{-1}) from the lunar occultation measurements of Snell and Schloerb (1985), and the areas of maximum integrated emission from the maps at 0.3 and −3.0 km s^{-1} taken from Fig. 6. In Fig. 8 it can also be seen that the high velocity emission position from the lunar occultation measurements coincides with the peak of integrated emission in the −3.0 km s^{-1} map. Our observations clearly show the presence of a shell structure in the southwest lobe of the L 1551 bipolar molecular outflow, as was hypothesised by Snell and Schloerb (1985).

The variation of the intensity of the CO emission with both velocity and position along the outflow axis was investigated for the observations made at UKIRT. Some of the relevant CO $J = 2$–1 and $J = 3$–2 spectra are shown in Fig. 4. Figure 9 shows a position-velocity plot of the CO $J = 3$–2 emission which is very similar to the equivalent plot for the CO $J = 1$–0 emission shown in Fig. 4 of Uchida et al. (1986). The main feature is the steady increase in the wing velocity (i.e. the velocity difference between the velocity of the ambient gas and that of the peak emission in the wing), with distance from IRS 5 up to about 3 arcmin from IRS 5 (2S 2W) and again from 3.5 arcmin from IRS 5 to about 5.5 arcmin from IRS 5 (4S 4W). Fridlund et al. (1984) also find a general increase of the wing velocity with distance from IRS 5 but they also observed that one peak of emission in the wing vanished at positions to the southwest of HH 29. This we do not see, but like Fridlund et al. (1984), we do see another peak of emission in the wing appear at velocities close to the ambient cloud velocity at positions southwest of both HH 29 and the faint nebulosity 35 arcsec southwest HH 29. From this, and also because of the low total integrated emission, low peak antenna temperature and the decrease in linewidth in both the $J = 3$–2 and $J = 2$–1 transitions of CO to the southwest of HH 29, it appears that the outflow may be interacting with something at or close to the position of HH 29. Fridlund et al. (1984) suggest that this could be a dense clump of ambient cloud material which, on excitation by the impact of the outflow, also manifests itself as a Herbig-Haro object. A consequence of the blocking of the outflow by a dense clump would be a sudden deceleration in the velocity of the outflowing gas and a reduction in the amount of material in the outflow immediately beyond the clump. However optical observations of HH 29 reported by Stocke et al. (1986) and the large proper motion of HH 29 measured by Cudworth and Herbig (1979) suggest that HH 29 is more likely to be an interstellar bullet rather than a dense clump of ambient material.

Our observations of the $J = 4$–3 transitions of HCO^+, $H^{13}CO^+$ and HCN at the position 2S 2W, which is 20 arcsec from HH 29, indicate the presence of either very dense gas ($> 10^5$ cm^3) or lower density gas with an unusually high abundance of these molecular species. The ratio of peak corrected antenna temperatures in the $J = 4$–3 transitions of HCO^+ to $H^{13}CO^+$ is 7 ± 1.5, which indicates that the HCO^+ line is optically thick with $\tau > 5$ for an isotopic abundance ratio of 40. The low intensity of the optically thick HCO^+ $J = 4$–3 emission could either be due to the HCO^+ $J = 4$ level being subthermally excited together with a large column density of HCO^+ along the line of sight, or be caused by beam dilution effects.if the HCO^+ emission originates in a number of small dense clumps which do not fill the beam area. The latter explanation indicates that extensive fragmentation of the denser gas is likely to be occurring. It is probable that the HCN and HCO^+ emission arise in different regions or as the result of different excitation processes as the line shapes are so different. The HCN $J = 4$–3 emission peaks at 3 km s^{-1} while both the HCO^+ and $H^{13}CO^+$ $J = 4$–3 lines peak at about 0 km s^{-1} as can be seen in Fig. 5. The HCO^+ line also has a second peak of emission at the ambient cloud

velocity. The detection of $H^{13}CO^+$ emission peaking at about $0\,km\,s^{-1}$ means that the double peaked structure observed in the HCO^+ $J = 4$–3 line is unlikely to be due to self absorption.

Large Velocity Gradient analysis of the CO $J = 3$–2 and $J = 2$–1 lines observed at UKIRT at this position at $0\,km\,s^{-1}$, assuming a source size of 1.5 arcmin in diameter (taken from the maps of the NRAO data), together with the values for the $J = 1$–0 transitions of CO and ^{13}CO taken from Snell et al. (1980) which were corrected for the appropriate source size, gives a fit within errors for an isotopic abundance ratio of 40 and a kinetic temperature of 25 K (Clark and Laureijs, 1986, and Edwards et al., 1986) for density of the exciting gas of $3\,10^3$ to $10^4\,cm^{-3}$. This differs from the density deduced in the paper by Richardson et al. (1985), primarily due to the assumed source size in this analysis being smaller and the use of more recent data for the CO $J = 3$–2 transition at the 2S 2W position. It is also possible that radiative transfer effects in this complicated region will mean that the use of the LVG analysis is inappropriate, giving unreliable results. If the velocity gradient is taken to be $80\,km\,s^{-1}\,pc^{-1}$ (Fridlund et al., 1984) the corresponding abundance of CO has an upper limit of $4\,10^{-5}$. For an isotopic abundance ratio of 89 the density of the exciting gas is between 10^3 and $10^4\,cm^{-3}$. The CO emission apparently comes from a region which has a density and temperature too low for the excitation of the $J = 4$–3 HCO^+ lines unless the HCO^+ has an abundance greater than that of CO as we have previously suggested. As the LVG analysis becomes very model dependent at high optical depths it is unlikely to be reliable in deriving the abundance of HCO^+ at this position. There is no $H^{13}CO^+$ emission at the ambient cloud velocity at 2S 2W and, although the profiles of the CO and HCO^+ lines observed at UKIRT are surprisingly similar in shape at this and other positions, the HCO^+ emission at the ambient cloud velocity is comparatively weaker than in the CO transitions observed. One reason for this difference is that the high velocity emission could occur in gas that has been shocked and the shock has enhanced the abundance of the HCO^+ (see White et al., 1986b, for observations of shocked gas in IC 443), particularly towards 2S 2W where $H^{13}CO^+$ has been detected. The passage of a relatively low shock velocity of about $10\,km\,s^{-1}$ can significantly enhance the abundance of HCO^+, as has been discussed by Mitchell and Deveau (1983). It is possible that HH 29 could be caused by a related shock process due to the interaction of the outflow with denser clumps of gas.

From these observations it appears that the HH 29 region is extremely complicated. It is possible that the interstellar medium at this position could consist of clumps of dense gas which give rise to the HCO^+ and $H^{13}CO^+$ emission, while the CO emission comes predominantly from a lower density interclump medium. This is a model that has been suggested for other sources including DR 21 (Richardson et al., 1986).

A second position of interest is 1.5S 2.5W where there is a hole in the position-velocity plots of the CO $J = 3$–2 emission in directions both parallel and perpendicular to the outflow axis at velocities between 0 and $5\,km\,s^{-1}$. There is emission at both the ambient cloud velocity and at velocities less than $0\,km\,s^{-1}$. This position is only 30 arcsec southwest of the high velocity lunar occultation point of Snell and Schloerb (1985) and is coincident with a small area of emission in the *R*, *V* and *I* wavebands (Snell et al., 1985). As this emission is weak in their H_α observations it is probably due to scattered light rather than shock excitation. The H_α radial velocity from observations made by Sarcander, Neckel and Elsasser (1985) show a change from -40 to $-72\,km\,s^{-1}$ at this position. There is obviously some interaction between the material giving rise to the optical emission and the molecular outflow at this position. One possibility is that the outflow is being bent around the clump of denser material that is scattering the light.

In order to make first order estimates of the properties of the flow source a simple model of a non-rotating outflow along a hyperboloidal shell of opening angle *v* has been derived to investigate the variation of the spectral profiles with position. The spectral lines are assumed to originate from four separate regions and have gaussian line shapes of variable widths. The four regions considered are: the background ambient cloud; the back and front of the shell which has thickness, *t*, and an optical depth which is proportional to the distance along the line of sight through the shell; and the gas within the shell which has an optical depth proportional to the distance along the line of sight between the two sides of the shell. No account of the effects of density, variation of optical depth with frequency or of radiative transfer within each region has been made. This is to allow simplicity with as few free parameters as possible. The gas within the shell has a constant outflow velocity, v_a, directed along the outflow axis. The velocity of the material within the shell is made up of a component of velocity tangential to the shell, v_t, and another component of constant velocity normal to the shell, v_n. The tangential velocity, v_t, consists of a constant component, v_{t1}, and a variable component, v_{t2}, which is proportional to the distance along the outflow axis, *x*. All velocities are in $km\,s^{-1}$. The axis of the shell is at an angle of inclination, *i*, to the plane of the sky. This is shown in Fig. 10. Initially the intensity of the emission for each of the regions, $I_n(v)$, at a given velocity, *v*, relative to the ambient cloud velocity is calculated using

$$I_n(v) = (hv/k) \cdot [\exp(hv/kT_n) - 1]^{-1} \cdot \exp[-(v - v_n)^2 \cdot 4 \ln 2/v^2_{FWHM}] \quad (1)$$

where v_n is the resultant velocity along the line of sight of the emitting gas relative to the ambient cloud velocity, v_{FWHM} is the

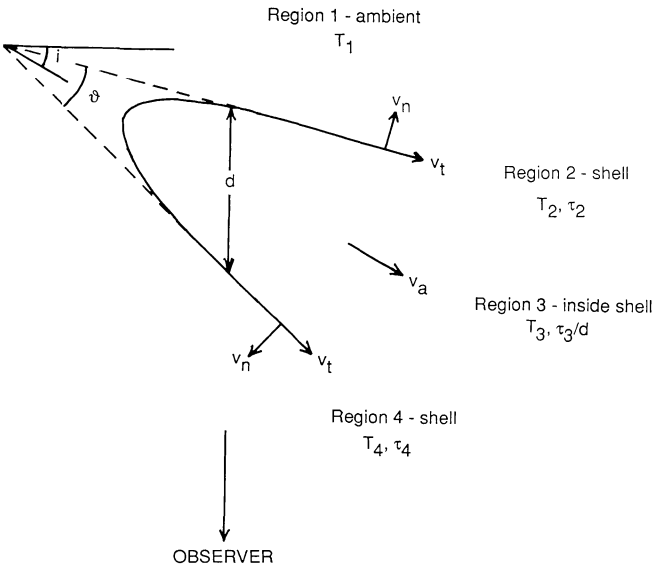

Fig. 10. Diagram to show parameters used in the hyperboloidal shell model of the outflow discussed in the text

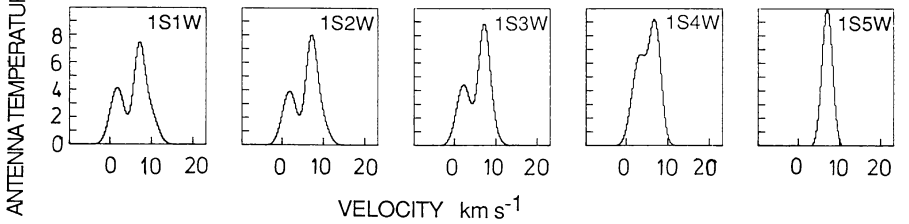

Fig. 11. A strip of five CO $J = 2$–1 spectra produced by the hyperboloidal shell model. The spectra are at one arcmin spacing along a line of constant declination

Table 2

Region	1	2 and 4	3
T(K)	15	25	35
V_{FWHM}(km s^{-1})	3	4	5
τ(pc^{-1})	–	5.5	0.1
v_a(km s^{-1})	–	–	12
v_n(km s^{-1})	–	1	–
v_{t1}(km s^{-1})	–	6	–
v_{t2}(km s^{-1} pc^{-1})	–	15	–
t(pc)	–	0.015	–

Notes: Ambient cloud velocity (V_{LSR}) = 6.7 km s^{-1}. $i = 15°$. $v = 9.7°$. Position angle of outflow axis = 225°

full width at half maximum of the gaussian line, and T_n is the excitation temperature of the line. Then the resultant intensity of emission at this velocity from all 4 regions is calculated using a simple radiative transfer equation

$$l_f(v) = l_1(v)\exp -(\tau_2+\tau_3+\tau_4) + l_2(v)[1-\exp(-\tau_2)]\exp -(\tau_3+\tau_4) + l_3(v)[1-\exp(-\tau_3)]\exp(-\tau_4) + l_4(v) \times [1-\exp(-\tau_4)] - l_{bb} \quad (2)$$

where τ_2 and τ_4 are the optical depths of the back and front of the shell, τ_3 is the optical depth of the material inside the shell along the line of sight and l_{bb} is the intensity of the background radiation. The optical depths per unit distance of the two sides of the shell are assumed to be the same.

Using the parameters given in Table 2 to model the CO $J = 2$–1 spectra we obtained the line of spectra shown in Fig. 11 at the same positions as the spectra shown in Fig. 3, which were observed at UKIRT, and close to the positions of the spectra observed at the NRAO 12 m telescope shown in Fig. 7. The values of the parameters T_n, i, v, t and the position angle of the outflow axis were chosen to be in agreement with observed values. There was not expected to be much agreement between the observed and model spectra towards the positions close to IRS 5 where the geometry of the shell has little resemblance to the actual situation which includes a dense disk. This may explain the discrepancy between the observed and model spectra towards the 1S 1W position, but we were able to produce a slight increase in intensity of the peak wing emission towards 1S 1W, compared to that towards 1S 2W, using the model. We found that the spectra produced by the model were very dependent on the exact positioning of the shell. One result of our modelling is that the acceleration of outflowing gas commented on by Fridlund et. al. (1984) and also seen in our observations can not be produced by a constant velocity outflow model where a decrease in the difference between the wing velocity and ambient cloud velocity is obtained. To give the observed increase there must be an acceleration of the outflowing gas.

To obtain the model spectra shown in Fig. 3 we had to use optical depths that were less than 1. Since the model does not convolve the spectra with the beamsize of the telescope that was used in making the observations, the low optical depths that the model required may be a consequence of the actual observations involving beam averaging effects over a clumpy medium.

We now summarise some of the main features of the L 1551 bipolar outflow. From the central source IRS 5 there is evidence of outflow on many scales. On the smallest scales of 0.001 to 0.01 pc are the radio and optical jets which are highly collimated. On much larger scales from 0.1 to 1 pc the molecular outflow is seen. Our observations, and those of Fridlund et al. (1984) and Uchida et al. (1986), show that the molecular gas in the southwest outflow lobe is accelerating out to at least 0.25 pc (5.5 arcmin) from IRS 5. The molecular outflow is not uniform and there is violent disruption of the outflow close to the position of HH 29 as is seen in our CO $J = 2$–1 and $J = 3$–2 observations and the detection of the $J = 4$–3 transitions of HCN, HCO^+ and $H^{13}CO^+$ at 2S 2W. We see another disruption of the outflow at the position 1.5S 2.5W.

One major result of our observations is the detection of a shell structure in the southwest outflow lobe which is between 0.03 to 0.07 pc thick. The shell structure could be due to ambient gas being swept up by a hot stellar wind, as been suggested by Snell, Loren and Plambeck (1980) and by Snell and Schloerb (1985). The similarity of the line profiles we have observed in the $J = 2$–1 and $J = 3$–2 transitions of CO and the $J = 4$–3 transition of HCO^+, particularly in the wings, suggest that velocity projection rather than optical depth effects is responsible for the differences in the spatial distribution of the low and high velocity blue shifted gas. This excludes the "viscous fluid in a pipe" model for L 1551 proposed by Levreault (1985) where optical depth effects should be seen. We have modelled the CO $J = 2$–1 spectra as arising from emission in an accelerating gas in a slowly expanding hyperboloid shell, which is inclined at 15° to the plane of the sky, with some further emission from hotter outflowing gas inside the shell.

Observations of redshifted emission towards certain areas of the southwest outflow lobe have been reported by Uchida et al. (1986). These results have been interpreted as evidence for a rotating shell which was predicted by the Sweeping-Magnetic-Twist model proposed by Uchida and Shibata (Uchida et al., 1986 and references therein). The shell structure is due to the magnetic field pattern formed by the contraction of the accretion disk. The relaxation of the magnetic twist, originally produced by the rotation of the accretion disk, drives out mass from the

surface of the disk giving rise to a helical outflow. Pudritz and Norman (1985) also propose a model which results in the rotation of the accelerating molecular outflow where the bipolar outflows are centrifugally driven hydromagnetic winds from molecular disks. The magnetic field enforces corotation of the outflowing gas with the disk out to the Alfvén surface, on scales ≥ 0.2 pc. By removing excess angular momentum of the gas in the disk, the hydromagnetic disk winds drive the accretion of the disk material onto a protostellar core. The outflowing molecular gas is collimated by effects of the wind's toroidal magnetic field. The disk wind also contains an ionized inner component, which is highly collimated by the pressure of the outflowing molecular gas.

We have detected redshifted emission in the northwestern part of the predominately blueshifted southwest outflow lobe in both the CO $J = 3$–2 and $J = 2$–1 transitions which could be due to rotation of the outflowing gas. The map of integrated redshifted CO $J = 2$–1 emission in Fig. 6 shows that the redshifted emission comes from a "shell" similar to that seen in the low velocity blueshifted emission although there is little redshifted emission to the south of the outflow axis, as would be expected from the likely direction of rotation of the outflow, which should be the same as that of the rotating disk (Kaifu et al., 1984) for both the Uchida and Shibata and the Pudritz and Norman models. The evidence of a shell structure from our CO observations favours the model of Uchida and Shibata but we cannot exclude that of Pudritz and Norman since although the concentration of gas along all the edges of the outflow is not predicted by their model, it is also not excluded. Similarly position velocity plots made in directions perpendicular to the outflow axis do not show the systematic velocity gradient expected for the corotating gas that is predicted by Pudritz and Norman but this could not be apparent in our observations due to low signal to noise and too few spectra. If the redshifted emission is due to rotation of the outflowing gas the models based on the collimation or confinement of isotopic winds by disks or density gradients will not be appropriate.

5. Conclusions

1. Our CO $J = 3$–2 and $J = 2$–1 observations show a shell structure which delineates the walls of the cavity of the southwest molecular outflow lobe of L 1551. The thickness of the shell is between 0.03 and 0.07 pc.

2. There is also some red-shifted emission to the north of the outflow axis that may be interpreted as evidence for rotation of the outflow.

3. We have detected the $J = 4$–3 transitions of HCO^+ and HCN at several positions. The $J = 4$–3 transition of $H^{13}CO^+$ was detected towards the position 2S 2W, close to HH 29.

4. The outflow is strongly disrupted close to HH 29. The HCO^+ emission is optically thick at this position and may have an enhanced abundance due to the effects of shocks on the interstellar chemistry. The high velocity CO emission at this position comes from gas for which LVG analysis gives a density of $3\,10^3$ to $10^4\,cm^{-3}$. The HCO^+ emission may come from dense clumps within this lower density gas.

5. We have modelled the outflow as an expanding hyperboloidal shell with an accelerating outflow. The opening angle of the outflow is 10°, the temperatures of the ambient gas, shell and inner shell gas are 15, 25 and 35 K respectively, and the shell gas has velocity components both normal and tangential to the shell surface, with the acceleration occuring in the tangential direction. The angle inclination of the axis of the shell to the plane of the sky is 15°.

6. Our observations, which suggest the presence of a rotating shell structure, may support the model proposed by Uchida and Shibata.

Acknowledgements. We thank the staff at ROE, UKIRT and the NRAO 12 m telescope for assistance with the observations, PATT and the NRAO for the allocations of telescope time, the SERC for travel grants and the funding of millimetre/submillimetre wave astronomy and receiver development at QMC, and the SERC for support for RR, KJR and MJG.

References

Batrla, W., Menten, K.M.: 1985, *Astrophys. J. Letters* **298**, L19
Bieging, J.H., Cohen, M., Schwartz, P.R.: 1984, *Astrophys. J.* **282**, 699
Bieging, J.H., Cohen, M., 1985, *Astrophys. J. Letters* **289**, L5
Clark, F.O., Laureijs, R.J.: 1986, *Astron. Astrophys. Letters* **154**, L26
Cohen, M., Bieging, J.H., Schwartz, P.R.: 1982 *Astrophys. J.* **253**, 707
Cohen, M., Schwartz, R.D.: 1983, *Astrophys. J.* **265**, 877
Cohen, M., Harvey, P.M., Schwartz, R.D., Wilking, B.A. 1984, *Astrophys. J.* **278**, 671
Cudworth, K.M., Herbig, G.: 1979, *Astron. J.* **84**, 548
Dent, W.R.F., Little, L.T., Sato, S. Ohishi, M. Yamashita, T.: 1985, *Monthly Notices Roy. Astron. Soc.* **217**, 217
Edwards, S., Strom, S.E., Snell, R.L., Jarrett, T.H., Beichman, C.A., Strom, K.M.: 1986, *Astrophys. J.* (in press)
Emerson, J.P., Harris, S., Jennings, R.E., Beichman, C.A., Baud, B.,
Beintema, D.A., Marsden, P.L., Wesselius, P.R.: 1984, *Astrophys. J. Letters* **278**, L49
Fridlund, C.V.M., Sandqvist, A., Nordh, H.L., Olofson, G.: 1984, *Astron. Astrophys. Letters* **137**, L17
Hodapp, K.-W.: 1984, *Astron. Astrophys.* **141**, 255
Kaifu, N., Suzuki, S., Hasegawa, T., Morimoto, M., Inatani, J., Nagane, K.,
Miyazawa, K., Chikada, Y., Kanzawa, T., Akabane, K.: 1984, *Astron. Astrophys.* **134**, 7
Knapp, G.R., Kuiper, T.B.H., Knapp, S.L., Brown, R.L.: 1976, *Astrophys. J.* **206**, 443
Kutner, M.L., Ulich, B.L.: 1981, *Astrophys. J.* **250**, 341
Levreault, R.M.: 1985, Ph. D. thesis, University of Texas Technical Report No. 85-1
Menten, K.M., Walmsley, C.M.: 1985, *Astron. Astrophys.* **146**, 369
Mirabel, I.F., Rodriguez, L.F., Cantó, J., Arnal, E.M.: 1985, *Astrophys. J. Letters* **294**, L39
Mitchell, G.F., Deveau, T.J.: 1983, *Astrophys. J.* **294**, 646
Mundt, R., Fried, J.W.: 1983, *Astrophys. J. Letters* **274**, L83
Mundt, R., Stocke, J., Strom, S.E., Strom, K.M., Anderson, E.R.: 1985, *Astrophys. J. Letters* **297**, L41
Nagata, T., Sato, S., Kobayashi, Y.: 1983, *Astron. Astrophys. Letters* **119**, L1
Pudritz, R.E., Norman, C.A.: 1986, *Astrophys. J.* **301**, 571

Richardson, K.J., White, G.J., Avery, L.W., Lesurf, J.C.G., Harten, R.H.: 1984, *Astrophys. J.* **290**, 637.
Richardson, K.J., White, G.J., Phillips, J.P., Avery, L.W.: 1986, *Monthly Notices Roy. Astron. Soc.* **219**, 167
Rodriguez, L.F., Cantó, J., Torrelles, J.M., Ho, P.T.P.: 1986, *Astrophys. J. Letters* **301**, L25
Sandqvist, Aa., Bernes, C.: 1980, *Astron. Astrophys.* **89**, 187
Sarcander, M., Neckel, Th., Elsasser, H.: 1985, *Astrophys. J. Letters* **288**, L51.
Snell, R.L., Loren, R.B., Plambeck, R.L.: 1980, *Astrophys. J. Letters* **239**, L17.
Snell, R.L.: 1981, *Astrophys. J. Suppl.* **45**, 121
Snell, R.L., Bally, J., Strom, S.E., Strom, K.M.: 1985, *Astrophys. J.* **290**, 587
Snell, R.L., Schloerb, F.P.: 1985, *Astrophys. J.* **295**, 490
Stocke, J., Strom, S.E., Strom, K.M., Hartigan, P.: 1986, Summer School on Interstellar Processes, July 3–7, Wyoming
Strom, K.M., Strom, S.E., Vrba, F.J.: 1976, *Astron. J.* **81**, 320
Strom, S.E., Strom, K.M., Grasdalen, G.L., Capps R.W., Thompson, D., 1985, *Astron. J.* **90**, 2575
Strom, S.E., Strom, K.M.: 1985, *Invited* Review at IAU Symp. 115.
Torrelles, J.M., Rodriguez, L.F., Cantó, J., Carral, P., Marcaide, J., Moran, J.M., Ho, P.T.P.: 1983, *Astrophys. J.* **274**, 214
Uchida, Y., Kaifu, N., Shibata, K., Hayashi, S.S., Hasegawa, T.: 1986, NRO Observatory Report No. 94, p. 25.
White, G.J., Monteiro, T.S., Richardson, K.J., Griffin, M.J., Rainey, R.: 1986a, *Astron. Astrophys.* **162**, 253
White, G.J., Rainey, R., Hayashi, S.S., Kaifu, N.: 1986, *Astron. Astrophys.* **173**, 337